

Title:

Achromatic polarization gratings as highly efficient thin-film polarizing beamsplitters for broadband light

Authors:

Chulwoo Oh and Michael J. Escuti

Affiliation:

North Carolina State University, Dept Electrical & Computer Engineering, Raleigh, NC (USA)

Presented At:

SPIE Optics & Photonics Conference, San Diego, CA (August 29, 2007)

Citation:

C. Oh and M.J. Escuti, "Achromatic polarization gratings as highly efficient thin-film polarizing beamsplitters for broadband light", *Proceedings of SPIE*, vol. **6682**, no. 668211 (2007).

Copyright 2007 Society of Photo-Optical Instrumentation Engineers.

This paper was published in Proceedings of SPIE Vol. 6682 and is made available as an electronic reprint with permission of SPIE. One print or electronic copy may be made for personal use only. Systematic or multiple reproduction, distribution to multiple locations via electronic or other means, duplication of any material in this paper for a fee or for commercial purposes, or modification of the content of this paper are prohibited.

Achromatic polarization gratings as highly efficient thin-film polarizing beamsplitters for broadband light

Chulwoo Oh and Michael J. Escuti

North Carolina State Univ, Dept Electrical & Computer Engineering, Raleigh, NC (USA)

ABSTRACT

We introduce and experimentally demonstrate an achromatic polarization grating (PG), which manifests high diffraction efficiency ($> 99.5\%$) over a broad range of spectrum. Unlike conventional phase gratings, this family of PGs has unique diffraction properties including three non-zero diffraction orders ($m = 0, \pm 1$) with up to 100% efficiency and strongly polarization sensitive first-order diffraction. It has long been recognized that these diffractive optical elements are useful for beamsplitting, polarimetry, displays, and more. A conventional (Circular-type) PG implemented with a spiraling, in-plane, linear birefringence has a modest spectral range ($\Delta\lambda/\lambda_0 \cong 6.8\%$) over which it possesses $> 99.5\%$ efficiency. We have identified a two-layer twisted PG structure that achieves achromatic diffraction that achieves a five-fold improvement of the high efficiency bandwidth ($\Delta\lambda/\lambda_0 \cong 34.3\%$). We have successfully implemented this structure with reactive mesogens (polymerizable liquid crystals) with a small amount of left- and right-hand chiral agents, and here report on its operation over nearly the entire range of visible light. We also investigated the behavior of the achromatic PG with the finite-difference time-domain method using an Open Source software package *WOLFSIM*, developed at NC State University, in order to evaluate the angular selectivity and the paraxial limit.

Keywords: achromatic diffraction, polarization grating, liquid crystals, reactive mesogens, holography, polarizing beamsplitter, circular polarizer

1. INTRODUCTION

Polarization measurement is important for a wide range of applications including spectropolarimetry, ellipsometry, remote sensing, biomedical imaging, optical communication, and quantum computing. Most traditional method for polarimetry is to measure the time-dependent signal transmitted through rotating quarter-waveplates or polarizers. These mechanical parts limit the detection speed and may cause severe vibration. An alternative way is to use polarizing beamsplitters separating the signal into the characteristic polarizations (i.e. orthogonal linear or orthogonal circular). However, conventional polarizing beamsplitters employing natural crystals such as quartz or polarization-sensitive thin-film structures generally have poor angular selectivity and strong wavelength dependency, which limits their applicability.

In recent years, polarization gratings (PGs)¹⁻⁴ have been introduced as efficient polarizing beamsplitters or optical switches.⁵⁻⁸ The most-studied PGs have its anisotropic profile consisting of a spiraling, constant-magnitude, linear birefringence (i.e. $\mathbf{n}(x) = [\sin(\pi x/\Lambda), \cos(\pi x/\Lambda), 0]$, where \mathbf{n} is a unity vector to describe the orientation of the linear birefringence and Λ is the effective optical period) as shown in Figure 1(a) and 1(b), which are also called Circular PGs⁹ due to their sensitivity of diffraction to the circular polarization. The ideal diffraction efficiency at normal incidence can be derived with Jones calculus¹⁰ (a reformulation of Refs.^{1,4}):

$$\eta_0 = \cos^2 \left(\frac{\pi \Delta n d}{\lambda} \right) \quad (1a)$$

$$\eta_{\pm 1} = \frac{1}{2} [1 \mp S'_3] \sin^2 \left(\frac{\pi \Delta n d}{\lambda} \right), \quad (1b)$$

Further author information: (Send correspondence to M.J.E.)
M.J.E.: E-mail: mjescuti@ncsu.edu

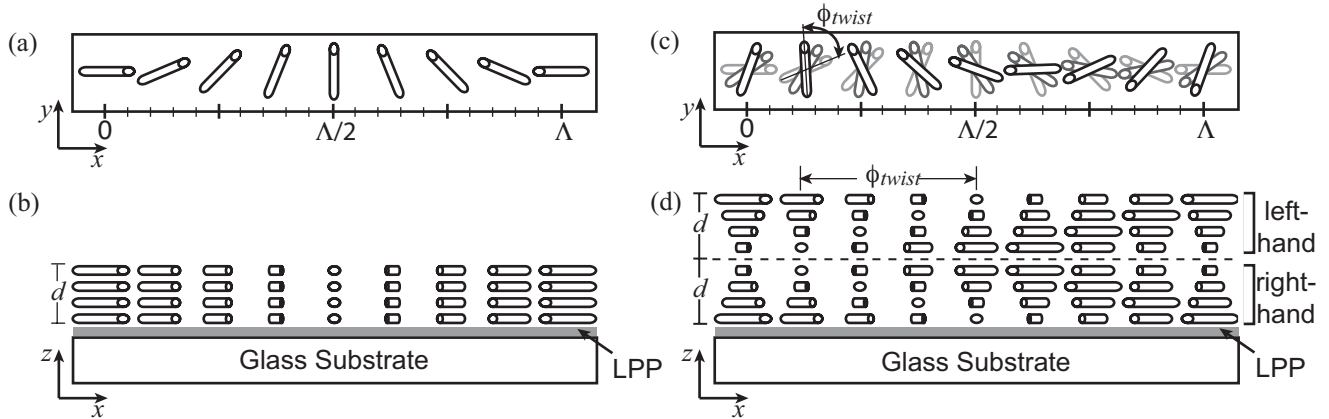


Figure 1. Polarization Gratings (PG) - Basic geometry of a Circular PG, (a) top view & (b) side view; achromatic PG with two chiral layers (opposite twist sense), (c) top view & (d) side view. Small bars depict the orientation of local linear birefringence.

where η_m is the diffraction efficiency of the m^{th} -order, λ is the vacuum wavelength of incident light, Δn is the linear birefringence, d is the grating thickness, and $S'_3 = S_3/S_0$ is the normalized Stokes parameter¹¹ corresponding to ellipticity of the incident polarization. Circular PGs manifest a unique combination of optical properties including only three orders (0 and ± 1) possible, up to 100% efficiency into a single order, orthogonal circular polarizations (left- and right-hand) of the first orders. Note that the diffraction behavior of Circular PGs depends modestly on the wavelength (through $\Delta n d/\lambda$ in Eqs. 1).

Most important benefits of Circular PGs over conventional diffraction gratings can be summarized as two features of diffraction properties: high efficiency up to $\sim 100\%$ and polarization sensitivity of the first order diffraction. Circular PGs have moderate diffraction bandwidth when compared with other gratings such as blazed gratings, Bragg gratings, and Raman-Nath gratings. For blazed and Bragg gratings, $\sim 100\%$ efficiency can be obtained in special conditions (i.e. $\theta_{inc} = \theta_{blazed}$ or θ_{Bragg}) and they generally have a fairly wide useful range of spectrum (i.e. from $\lambda_0/2$ to $3\lambda_0/2$), which is somewhat larger than that of Circular PGs (i.e. from $3\lambda_0/4$ to $5\lambda_0/4$). However, diffraction efficiencies of both blazed and Bragg gratings are highly sensitive to incident angle variation, which often requires mechanical motion or special treatment to match the optimal conditions for the maximum diffraction. Up to now, no diffraction gratings have been reported to have high efficiencies (close to 100%) in a wide range of spectrum. Although Tervo et al.¹² reported an achromatic design of the diffraction elements using subwavelength features, there is no practical method to implement such a kind of gratings.

Here, we introduce and demonstrate an achromatic polarization grating that exhibits high diffraction efficiencies over a wide range of spectrum. Our approach is based on the retardation compensation, where two low-twist, chiral PG layers are stacked with opposite twist sense. Figure 1(c) and 1(d) illustrates the layout of the achromatic PG design. In Section 2, we will find the analytical solutions for general diffraction properties of an ideal achromatic PG (assuming infinite grating period and normal incidence) using the Jones matrix analysis. In Section 3, we also apply the finite-difference time-domain (FDTD) method^{13,14} using *WOLFSIM*,¹⁵ which is an open-source software package developed for periodic anisotropic media at NC State University. The angular selectivity and paraxial limit of diffraction will be discussed as well as basic diffraction properties of the achromatic PG. Finally, in Section 4, we present the experimental demonstration of the achromatic PG as reactive mesogen (RM) films with small amount of left- and right-hand chiral dopants.

2. THEORETICAL FOUNDATION OF ACHROMATIC POLARIZATION GRATINGS

In order to derive the governing expressions for the achromatic PG, we employ Jones matrix analysis.¹⁶ We see the diffraction efficiencies and electric fields for an achromatic PG consisting of two symmetric chiral Circular PGs with opposite twist sense. We will find the generic equations for a single chiral Circular PG and then we will look for the solutions for the achromatic PG.

A Circular PG is formed of the retardation film (or the waveplate) with periodically varying anisotropy. The Jones matrix for a Circular PG can be expressed as

$$\mathbf{T}_{PG} = \mathbf{R}(-\phi) \begin{bmatrix} e^{-i\Gamma} & 0 \\ 0 & e^{i\Gamma} \end{bmatrix} \mathbf{R}(\phi) \quad (2)$$

where $\Gamma = \pi\Delta nd/\lambda$ is the retardation, \mathbf{R} is the rotation matrix, and $\phi = \phi(x) = \pi x/\Lambda$.

Now we consider a Circular PG with additional rotational variation along the thickness, often called twist in liquid crystals. The Jones matrix for a stack of multiple thin layers (N) of the Circular PG with a small phase shift $\Delta\phi$ (or a twist) in the azimuth can be written as¹⁷

$$\mathbf{T}_{PG,twist} = \prod_{m=1}^N \mathbf{R}(-m\Delta\phi) \mathbf{T}_{PG}(\Delta\Gamma) \mathbf{R}(m\Delta\phi) \quad (3)$$

where N is the number of PG layers, $\Delta\Gamma = \Gamma/N$ is the retardation of each thin layer, and $\phi_{twist} = N\Delta\phi$ is the total twist angle. The achromatic PG is composed of a stack of two chiral Circular PGs with opposite twist sense. The Jones matrix \mathbf{T}_{APG} can be obtained simply by multiplying the Jones matrices for two Circular PGs:

$$\mathbf{T}_{APG} = \mathbf{T}'_{PG,twist} \mathbf{T}_{PG,twist} \quad (4)$$

Note that the Jones matrix \mathbf{T}'_{APG} for the second Circular PG can be obtained by substituting $\phi' = \phi + \phi_{twist}$ and $\phi'_{twist} = -\phi_{twist}$ in Eqs. 2 and 3.

After considerable mathematical efforts (for more details, refer to Appendix A), the final expressions for diffraction efficiencies of the achromatic PG can be obtained as follows

$$\eta_0 = \left[\cos^2 X + (\phi_{twist}^2 - \Gamma^2) \left(\frac{\sin X}{X} \right)^2 \right]^2 \quad (5a)$$

$$\Sigma\eta_{\pm 1} = 1 - \left[\cos^2 X + (\phi_{twist}^2 - \Gamma^2) \left(\frac{\sin X}{X} \right)^2 \right]^2 \quad (5b)$$

where $\Gamma = \pi\Delta nd/\lambda$ and $X = \sqrt{\phi_{twist}^2 + \Gamma^2}$. We omit the individual expressions for the first order efficiencies ($\eta_{\pm 1}$) because of complexity. Interestingly, diffraction efficiencies (η_0 or $\Sigma\eta_{\pm 1}$) only depend on retardation (Γ) and the twist angle (ϕ_{twist}). In addition, the two first orders have orthogonal circular polarizations as normal

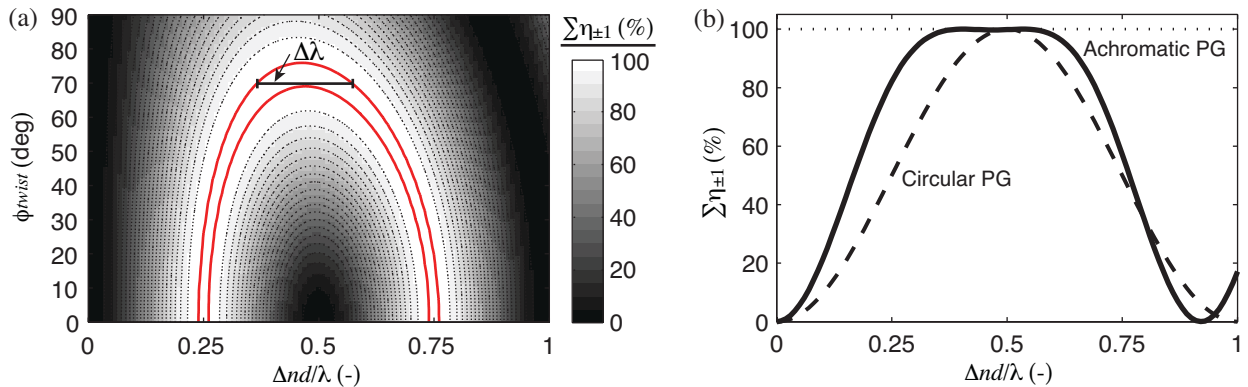


Figure 2. Calculated diffraction efficiencies of the achromatic PG composed of two chiral Circular PGs with opposite twist sense: (a) Spectral range for high efficiency ($\Sigma\eta_{\pm 1} \geq 99.5\%$, enclosed area); (b) Diffraction spectra for $\phi_{twist} = 70^\circ$. Gray scale levels depict diffraction efficiency and the bandwidth $\Delta\lambda/\lambda_{center}$ is maximized at the region shown. Note that d is the thickness of each grating layer and the final grating thickness is $2d$.

Circular PGs while the polarization of the 0-order remains same as the incident polarization. We can interpret that the polarization effect of twist is canceled out by two chiral layers with opposite twist sense.

To quantitatively evaluate the diffraction bandwidth, we introduce the spectral range $\Delta\lambda$ (units of wavelength) for high diffraction efficiency as the range of wavelengths over which the total first-order diffraction $\Sigma\eta_{\pm 1}$ is $\geq 99.5\%$. The normalized bandwidth $\Delta\lambda/\lambda_{center}$ (units of %) is defined as the ratio of the spectral range to its center wavelength λ_{center} . Circular PGs have a modest diffraction bandwidth given by $\Delta\lambda/\lambda_{center} \cong 6.8\%$.

Figure 2(a) shows a map of diffraction efficiency ($\Sigma\eta_{\pm 1}$) as a function of the normalized retardation ($\Delta nd/\lambda$) and the twist angle (ϕ_{twist}). The spectral range $\Delta\lambda$ for $\Sigma\eta_{\pm 1} \geq 99.5\%$ is highlighted in the figure. The maximum bandwidth $\Delta\lambda/\lambda_{center} \cong 34.3\%$ is found when $\phi_{twist} = 70^\circ$. Note that this is a five-fold enhancement in the maximum diffraction bandwidth as compared with Circular PGs. For twist angles smaller than 70° , the diffraction bandwidth increases gradually as the twist angle increases. On the other hand, the diffraction bandwidth decreases drastically for higher twist angles. The achromaticity of the diffraction can be explained by the counter chromatic dispersions of retardation by linear birefringence and induced circular birefringence due to twist. The former becomes larger for shorter wavelengths while the latter becomes larger for longer wavelengths and vice versa. When $\Delta nd = \lambda_0/2$ and $\phi_{twist} = 70^\circ$, the retardation compensation occurs by balancing out both effects and the achromatic diffraction is achieved. Figure 2(b) shows a comparison of diffraction spectra of the achromatic PG with that of the Circular PG.

The polarization sensitivity of the first orders was also calculated. As shown in Figure 3(a), first-order diffraction is sensitive to the ellipticity angle χ of the incident polarization. As this ellipticity changes, diffraction power is redistributed between the ± 1 -orders: for example, the first-orders have the same diffraction efficiency for unpolarized/linear polarization input, while all of the diffracted light appears in only one of the first-orders for circular polarization input (selected by handedness). Figure 3(b) shows the first-order efficiencies $\eta_{\pm 1}$ at the halfwave thickness $\Delta nd = \lambda/2$ with respect to the ellipticity angle χ . Note that the 0-order efficiency is independent to the incident polarization.

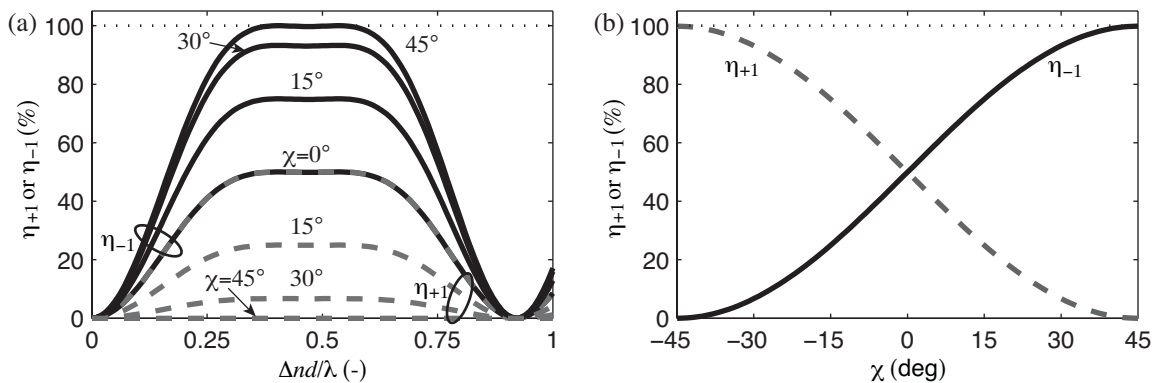


Figure 3. Polarization sensitivity of the first order diffraction of the achromatic PG with $\phi_{twist} = 70^\circ$: (a) Diffraction spectra of the +1-order (dashed-line) and the -1-order (solid-line) for different ellipticity angles χ ; (b) First order efficiencies at $\Delta nd = \lambda/2$ as a function of χ .

3. NUMERICAL STUDIES OF ACHROMATIC POLARIZATION GRATINGS

In this Section, we simulate the achromatic PG with an Open Source finite-difference time-domain (FDTD) tool¹⁵ to model the angular selectivity and paraxial limit of the achromatic PG diffraction. Since the Jones matrix analysis is only valid within the paraxial approximations (i.e. normal incidence and small diffraction angles), Eqs. 5 for diffraction efficiencies may not be applicable at oblique incidence and small grating periods close to the wavelength (i.e. $\Lambda/\lambda \approx 1$). *WOLFSIM* (Wideband Optical FDTD Simulator)¹⁵ provides an efficient optical simulation tool especially for periodic anisotropic media such as polarization gratings. *WOLFSIM* applies the modified split-field FDTD method¹⁸ to simulate the electromagnetic propagation/scattering in arbitrary

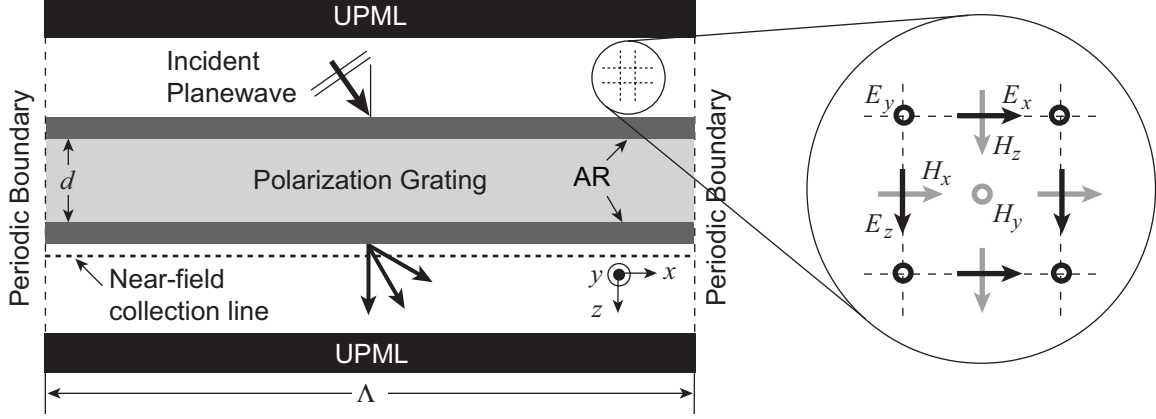


Figure 4. Schematics of the 2D FDTD simulation space. The inset figure shows the field distribution on square-grid lattices. Note that the x -width is determined by the grating period.

anisotropic media at a general angle of incidence. Recently,⁹ we reported intensive numerical studies of the PG diffraction using *WOLFSIM*.

Figure 4 illustrates the geometry of the 2D simulation space for the analysis of the achromatic PG. The grating structure is located in the middle of the square grid space by defining material parameters at every grid point. For the Circular PG with a twist, the permittivity tensor $\tilde{\epsilon}$ can be written as

$$\tilde{\epsilon} = \begin{bmatrix} \epsilon_{xx} & \epsilon_{xy} & \epsilon_{xz} \\ \epsilon_{yx} & \epsilon_{yy} & \epsilon_{yz} \\ \epsilon_{zx} & \epsilon_{zy} & \epsilon_{zz} \end{bmatrix} = \mathbf{R}^{-1}(\phi) \begin{bmatrix} n_{ex}^2 & 0 & 0 \\ 0 & n_{or}^2 & 0 \\ 0 & 0 & n_{or}^2 \end{bmatrix} \mathbf{R}(\phi), \quad (6)$$

where n_{or} and n_{ex} are the refractive indices observed by linearly polarized light in the ordinary (perpendicular) and extra-ordinary (parallel) directions of the uniaxial anisotropy (linear birefringence is defined as $\Delta n = n_{ex} - n_{or}$). \mathbf{R} is a rotation matrix where $\phi(x)$ is the azimuth angle measured from the x -axis:

$$\mathbf{R}(\phi) = \begin{bmatrix} \cos(\phi) & -\sin(\phi) & 0 \\ \sin(\phi) & \cos(\phi) & 0 \\ 0 & 0 & 1 \end{bmatrix}, \quad (7)$$

where $\phi(x) = \pi x/\Lambda + (z/d)\phi_{twist}$.

The simulation space is reduced to only one grating period by applying the periodic boundary conditions. The remaining two boundaries are truncated by the uniaxial perfectly matched absorbing layers (UPMLs¹⁹) to minimize non-physical reflection at the boundaries. To minimize the Fresnel losses at the air-grating interfaces, gradient-index anti-reflection coatings²⁰ are applied. A Gaussian pulse centered at the wavelength of interest is excited in front of the grating structure for wideband analysis from a single simulation. The near-field values right after the grating were sampled at every time step and transformed in the far-field. Finally, the discrete Fourier transformation is performed to extract the spectral information. We also calculate the Stokes parameters for each diffracted order to examine the polarization states.

Figure 5(a) shows the diffraction spectra as a function of $\Delta nd/\lambda$ of the achromatic PG when $\phi_{twist} = 70^\circ$. We modeled the material parameters as $n_{or} = 1.4$ and $\Delta n = 0.2$. The grating period was selected to $\Lambda = 20\lambda_0$ (λ_0 is the center wavelength of the Gaussian pulse) to ensure the grating operating well below the paraxial limit. The grating thickness was fixed for $\Delta nd = \lambda_0/2$. The polarization sensitivity of the first order efficiencies was also tested as shown in Figure 5(b). As expected, excellent agreement between FDTD results and the analytic solutions is found in both cases.

We also evaluated the angular selectivity of the achromatic PG diffraction from a series of simulations with varying the incident angle from -45° to 45° . The Gaussian-pulse was again used as the source, with right-handed circular polarization input (only -1 -order exists at normal incidence). Figure 6(a) shows the -1 -order efficiency

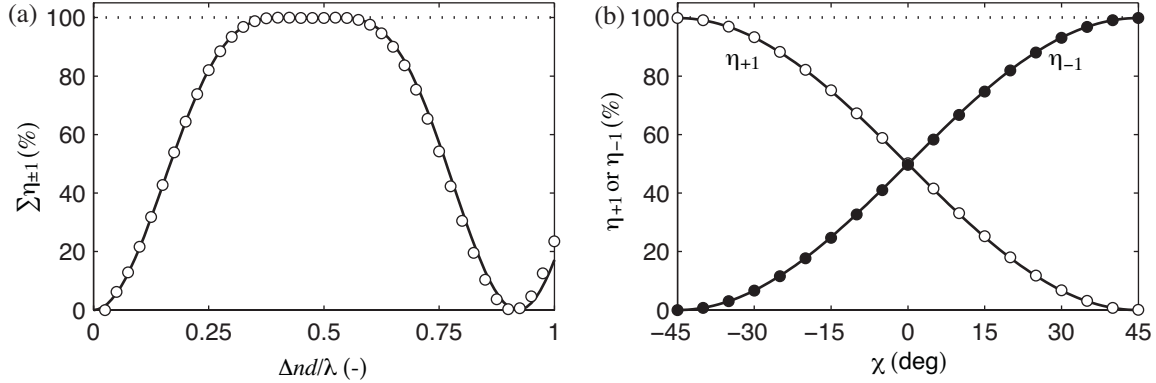


Figure 5. Diffraction behavior of the achromatic PG numerically calculated (\circ , \bullet) and analytically estimated (curves) using Eq. 5 when $\phi_{twist} = 70^\circ$: (a) Diffraction spectra of the first order efficiency ($\Sigma\eta_{\pm 1}$) as a function of $\Delta nd/\lambda$; (b) Polarization sensitivity of the first order diffraction ($\eta_{\pm 1}$) with respect to the ellipticity angle χ of the incident polarization.

(η_{-1}) as a function of $\Delta nd/\lambda$ for various incident angles. For small angles of incidence θ_{inc} , only the -1 -order has appreciable power ($\approx 100\%$) and manifests a nearly perfect right-handed circular polarization ($S'_3 \simeq 1$). A modest decrease of η_{-1} is found as the incident angle increases. The degradation in efficiency become larger for longer wavelengths. The angular selectivity is slightly asymmetric with respect to $\theta_{inc} = 0^\circ$. Degradation in the efficiency is faster for positive incident angles than for negative angles. We consider all of these off-axis effects as being primarily related to a change in the effective optical path length experienced by the incident lightwave as θ_{inc} increases.

For compact and efficient systems, a large angular dispersion is preferred. However, since polarization gratings operate within the paraxial domain, large diffraction angles and high efficiencies are not always available. We have found that the paraxial limit for Circular PGs can be effectively described by a dimensionless parameter^{9,21} ρ as $\rho \leq 1$:

$$\rho = \frac{2\lambda^2}{\bar{n}\Delta n\Lambda^2}, \quad (8)$$

where $\bar{n} = \frac{1}{2}(n_{or} + n_{ex})$ is the average refractive index of the media. More details on the Circular PG diffraction beyond the paraxial approximation can be found in Ref.⁹ We evaluate the diffraction properties of the achromatic PG close to the paraxial limit where $\rho \simeq 1$. Since ρ is proportional to a square of the ratio Λ/λ_0 , we calculated the diffraction efficiency with varying Λ/λ_0 from 1 to 10.

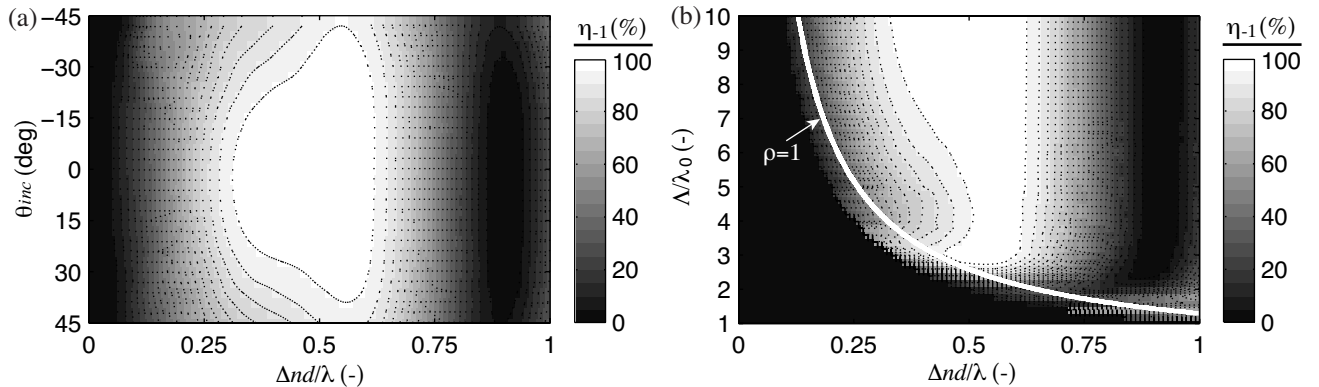


Figure 6. Diffraction behavior of the achromatic PG ($\phi_{twist} = 70^\circ$) at oblique incidence and near the paraxial limit. Diffraction spectra is plotted as a function of (a) incident angle θ_{inc} and (b) the ratio Λ/λ . Gray scale levels depict simulated diffraction efficiency of one of the first orders (η_{-1}). ($\Lambda = 20\lambda_0$ for part (a) and $n_o = 1.4$, $\Delta n = 0.2$, and $\Delta nd = \lambda_0/2$ for both cases)

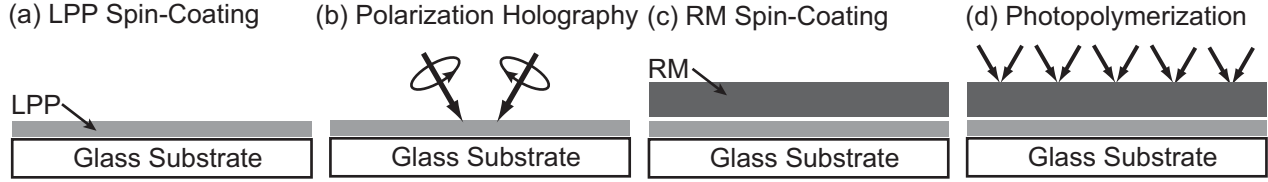


Figure 7. Fabrication steps of reactive mesogen PGs using polarization holography and photo-alignment techniques.

Figure 6(b) shows a map of the diffraction efficiency (η_{-1}) as a function of $\Delta nd/\lambda$ and Λ/λ_0 . The spectral range for high efficiency decreases as the ratio Λ/λ_0 approaches to a unity. Diffraction at longer wavelengths are more sensitive to the change of Λ/λ and the efficiency decreases more rapidly while high efficiencies are still available at shorter wavelengths until it reaches the paraxial limit (i.e. $\rho \approx 1$, outlined). It should be note that the achromatic PG exhibits diffraction properties exceeding far beyond conventional Circular PGs with respect to the angular selectivity and paraxial limit.

4. ACHROMATIC PG USING REACTIVE MESOGENS

We also experimentally demonstrated the achromatic PG formed as a reactive mesogen (RM) film by polarization holography and photo-alignment techniques.^{22,23} We have recently¹⁰ fabricated defect-free RM PGs (conventional) with ultra-high efficiency and low scattering by materials and processing optimization. The key of the fabrication technique is the use of photo-alignment materials that allow the separation of hologram recording and grating structure amplification. As shown in Figure 7, fabrication of reactive mesogen PGs proceeds with following four basic steps: first, a thin layer of photo-alignment material is coated on a glass substrate (Figure 7(a)); second, the substrate is exposed with two coherent beams from a laser with orthogonal circular polarizations at a small angle, leading to polarization interference with a constant intensity (Figure 7(b)); third, the RM mixture is coated on the photo-alignment layer and made to be align according to the surface pattern (Figure 7(c)); finally, the RM layer is photopolymerized with a blanket ultraviolet exposure to permanently fix the large structured optical anisotropy (Figure 7(d)).

We use this basic fabrication also for the achromatic PG. In particular, we utilized a linear-photopolymerizable polymer²⁴ (LPP) ROP-103 (Rolic) as a photo-alignment material. The surface alignment pattern with a period of $\Lambda = 8.5\mu\text{m}$ was recorded in the LPP layer by orthogonal circular polarized beams from a HeCd laser (325nm). After LPP exposure, RM films were deposited on the LPP-coated substrate by spin-coating until it reached the

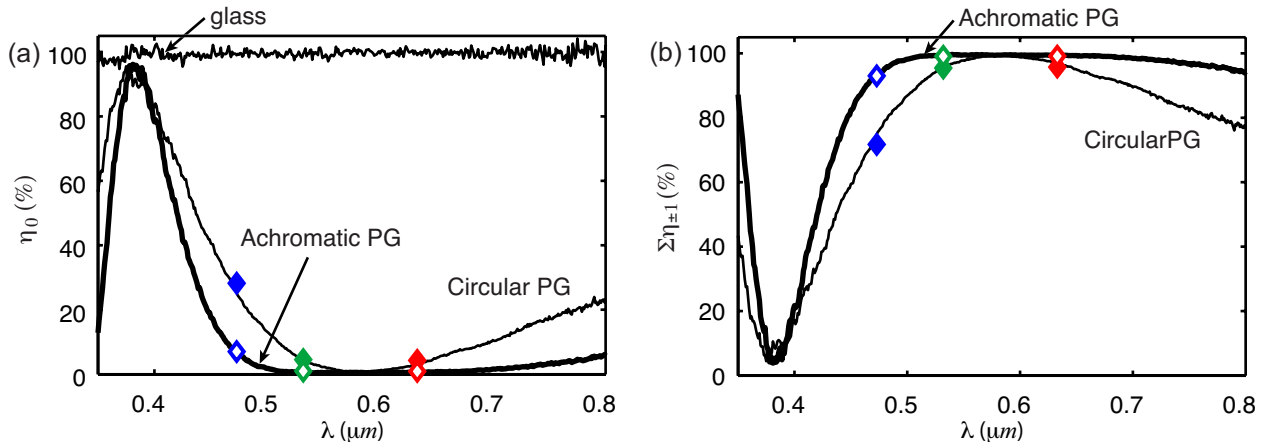


Figure 8. Experimental results from the achromatic PG ($\Lambda = 8.5\mu\text{m}$) as implemented with reactive mesogens: (a) the 0- order efficiency spectra; (b) estimated first-order efficiency spectra, calculated from the 0-order ($\Sigma\eta_{\pm 1} \approx 1 - \eta_0$). A clean glass slide is shown as reference in part (a). Diffraction spectra (experimentally measured) of a conventional RMPG are shown for comparison. Exact efficiencies (diamonds) at three wavelengths were measured with red (633nm), green (532nm), and blue (473nm) lasers for both the achromatic PG (white face-color) and the conventional PG (colored-face).

required thickness. The first RM layer was a mixture composed of RMS03-001 (Merck, $\Delta n \simeq 0.159$ at $589nm$) with small amount (0.25%) of chiral dopant CB15 (Merck, right-handed), chosen so that the RM layer reached the half-wave thickness ($\Delta nd = \lambda/2$) and $\phi_{twist} = 70^\circ$. The second RM layer was deposited directly on the top of the first, and was composed of RMS03-001 doped with a small amount (0.34%) of a different chiral agent, ZLI-811 (Merck, left-handed), subject to the same thickness and twist angle. Note that the final grating thickness was $\sim 2d$, because two layers were stacked (each with the half-wave thickness).

Figure 8(a) shows the 0-order efficiency spectra of both samples of the Circular PG and the achromatic PG, measured with a spectrophotometer. Note that the spectra of the transmittance of a clean glass slide ($\sim 100\%$) was measured under the identical conditions to the PGs. The spectra of the diffraction efficiency was estimated as $\Sigma \eta_{\pm 1} \approx 1 - \eta_0$, plotted in Figure 8(b), because of the difficulty of its direct measurement. Exact efficiencies were measured at red ($633nm$), green ($532nm$), and blue ($453nm$) laser wavelengths, which conclusively confirm the estimated efficiencies in Figure 8(b). As expected from FDTD simulation results, a noticeable improvement in the diffraction bandwidth is found. Note that the diffraction efficiency is defined as $\eta_m = I_m/I_{REF}$, where I_m is the measured intensity of the m^{th} transmitted diffracted order, and where I_{REF} is a reference transmission intensity for a glass substrate. Note that we roughly measured the incoherent scattering as 2% or less above $400nm$, by comparing the diffracted spectra to the clean glass slide.

5. CONCLUSIONS

We have designed and demonstrated an achromatic PG formed in polymerizable liquid crystals, which achieves ultra-high efficiency over a broad spectral range. Analytic expressions for basic diffraction properties of the achromatic PG were derived using the Jones matrix analysis. We further investigated diffraction behavior at oblique incidence and beyond paraxial limit using FDTD simulations. Finally, we experimentally realized a high-quality achromatic PG using reactive mesogens with improved bandwidth (almost over the entire visible range) for high diffraction efficiency and low scattering. This thin-film achromatic PG offers substantially more functional control than any other diffraction grating over the direction, intensity, and polarization state of the transmitted light (for a wide spectral bandwidth), and has high potential to benefit many applications, including remote sensing, biomedical imaging, optical communications, quantum computing, and more.

ACKNOWLEDGMENTS

The authors gratefully acknowledge support from the National Science Foundation (grant ECCS-0621906).

APPENDIX A. JONES MATRIX ANALYSIS FOR ACHROMATIC PG

The Jones matrix for a Circular PG can be expressed as

$$\mathbf{T}_{PG} = \mathbf{R}(-\phi) \begin{bmatrix} e^{-i\Gamma} & 0 \\ 0 & e^{i\Gamma} \end{bmatrix} \mathbf{R}(\phi) \quad (9)$$

where $\Gamma = \pi \Delta nd / \lambda$ is the retardation, \mathbf{R} is the rotation matrix, and $\phi = \phi(x) = \pi x / \Lambda$.

The Circular PG with a twist can be approximated as a stack of multiple (N) thin Circular PG layers with a small phase shift $\Delta\phi$ in the azimuth. The Jones matrix for this stratified grating structure can be written as

$$\begin{aligned} \mathbf{T}_{PG,twist} &= \prod_{m=1}^N \mathbf{R}(-m\Delta\phi) \mathbf{T}_{PG}(\Delta\Gamma) \mathbf{R}(m\Delta\phi) \\ &= \mathbf{R}(-\phi_{twist}) [\mathbf{T}_{PG}(\Delta\Gamma) \mathbf{R}(\Delta\phi)]^N \end{aligned} \quad (10)$$

where N is the number of Circular PG layers, $\Delta\Gamma = \Gamma/N$ is the retardation of each layer, and $\phi_{twist} = N\Delta\phi$ is the total twist angle.

Now we introduce an auxiliary matrix $\mathbf{W} = \mathbf{T}_{PG} \mathbf{R}(\Delta\phi)$:

$$\mathbf{W} = \begin{bmatrix} W_{11} & W_{12} \\ W_{21} & W_{22} \end{bmatrix}, \quad (11)$$

where

$$W_{11} = (e^{-i\Delta\Gamma} \cos^2(\phi) + e^{i\Delta\Gamma} \sin^2(\phi)) \cos(\Delta\phi) - (e^{-i\Delta\Gamma} - e^{i\Delta\Gamma}) \sin(\phi) \cos(\phi) \sin(\Delta\phi) \quad (12a)$$

$$W_{12} = (e^{-i\Delta\Gamma} \cos^2(\phi) + e^{i\Delta\Gamma} \sin^2(\phi)) \sin(\Delta\phi) + (e^{-i\Delta\Gamma} - e^{i\Delta\Gamma}) \sin(\phi) \cos(\phi) \cos(\Delta\phi) \quad (12b)$$

$$W_{21} = -(e^{-i\Delta\Gamma} \sin^2(\phi) + e^{i\Delta\Gamma} \cos^2(\phi)) \sin(\Delta\phi) + (e^{-i\Delta\Gamma} - e^{i\Delta\Gamma}) \sin(\phi) \cos(\phi) \cos(\Delta\phi) \quad (12c)$$

$$W_{22} = (e^{-i\Delta\Gamma} \sin^2(\phi) + e^{i\Delta\Gamma} \cos^2(\phi)) \cos(\Delta\phi) + (e^{-i\Delta\Gamma} - e^{i\Delta\Gamma}) \sin(\phi) \cos(\phi) \sin(\Delta\phi) \quad (12d)$$

As $N \rightarrow \infty$, we can simplify W_{11} as follows

$$W_{11} \cong \cos(\Delta\phi) - i(\Delta\Gamma) \cos(2\phi) \quad (13a)$$

$$W_{12} \cong \Delta\phi - i(\Delta\Gamma) \sin(2\phi) \quad (13b)$$

$$W_{21} \cong -\Delta\phi - i(\Delta\Gamma) \sin(2\phi) \quad (13c)$$

$$W_{22} \cong \cos(\Delta\phi) + i(\Delta\Gamma) \cos(2\phi) \quad (13d)$$

Using Chebychev's identity, we can find a matrix $\mathbf{W}' = \mathbf{W}^N$ as follows

$$\begin{aligned} \mathbf{W}' &= \begin{bmatrix} W'_{11} & W'_{12} \\ W'_{21} & W'_{22} \end{bmatrix} \\ &= \begin{bmatrix} \frac{W_{11} \sin(NZ) - \sin(N-1)Z}{\sin(Z)} & \frac{W_{12} \sin(NZ)}{\sin(Z)} \\ \frac{W_{21} \sin(NZ)}{\sin(Z)} & \frac{W_{22} \sin(NZ) - \sin(N-1)Z}{\sin(Z)} \end{bmatrix} \end{aligned} \quad (14)$$

where W'_{ij} is the (i, j) component of \mathbf{W}' and $Z = \cos^{-1} \left[\frac{1}{2}(W_{11} + W_{22}) \right]$.

We can further simplify \mathbf{W}' using approximations: as $N \rightarrow \infty$, $\sin(NZ)/NZ \cong \sin X/X$ and $\cos(NZ) \cong \cos X$, where $X = \sqrt{\phi^2 + \Gamma^2}$.

$$W'_{11} \cong \cos(X) - i\Gamma \cos(2\phi) \left[\frac{\sin(X)}{X} \right] \quad (15a)$$

$$W'_{12} \cong [\phi_{twist} - i\Gamma \sin(2\phi)] \left[\frac{\sin(X)}{X} \right] \quad (15b)$$

$$W'_{11} \cong -[\phi_{twist} + i\Gamma \sin(2\phi)] \left[\frac{\sin(X)}{X} \right] \quad (15c)$$

$$W'_{11} \cong \cos(X) + i\Gamma \cos(2\phi) \left[\frac{\sin(X)}{X} \right] \quad (15d)$$

Substituting \mathbf{W}' into Eq. 10, we finally get the Jones matrix for the PG with twist:

$$\mathbf{T}_{PG,twist} = \begin{bmatrix} T_{11} & T_{12} \\ T_{21} & T_{22} \end{bmatrix} = \mathbf{R}(-\phi_{twist}) \mathbf{W}' \quad (16)$$

where T_{ij} is the (i, j) component of $\mathbf{T}_{PG,twist}$:

$$T_{11} = \cos(\phi_{twist}) \cos(X) + \phi_{twist} \sin(\phi_{twist}) \left[\frac{\sin(X)}{X} \right] - i\frac{\Gamma}{2} \left[\frac{\sin(X)}{X} \right] e^{i\phi_{twist}} e^{i2\phi} - i\frac{\Gamma}{2} \left[\frac{\sin(X)}{X} \right] e^{-i\phi_{twist}} e^{-i2\phi} \quad (17a)$$

$$T_{12} = -\sin(\phi_{twist}) \cos(X) + \phi_{twist} \cos(\phi_{twist}) \left[\frac{\sin(X)}{X} \right] - \frac{\Gamma}{2} \left[\frac{\sin(X)}{X} \right] e^{i\phi_{twist}} e^{i2\phi} + \frac{\Gamma}{2} \left[\frac{\sin(X)}{X} \right] e^{-i\phi_{twist}} e^{-i2\phi} \quad (17b)$$

$$T_{21} = \sin(\phi_{twist}) \cos(X) - \phi_{twist} \cos(\phi_{twist}) \left[\frac{\sin(X)}{X} \right] - \frac{\Gamma}{2} \left[\frac{\sin(X)}{X} \right] e^{i\phi_{twist}} e^{i2\phi} + \frac{\Gamma}{2} \left[\frac{\sin(X)}{X} \right] e^{-i\phi_{twist}} e^{-i2\phi} \quad (17c)$$

$$T_{22} = \cos(\phi_{twist}) \cos(X) + \phi_{twist} \sin(\phi_{twist}) \left[\frac{\sin(X)}{X} \right] + i\frac{\Gamma}{2} \left[\frac{\sin(X)}{X} \right] e^{i\phi_{twist}} e^{i2\phi} + i\frac{\Gamma}{2} \left[\frac{\sin(X)}{X} \right] e^{-i\phi_{twist}} e^{-i2\phi} \quad (17d)$$

where $X = \sqrt{\phi_{twist}^2 + \Gamma^2}$. The Jones matrix $\mathbf{T}_{PG,twist}$ can be split into three matrices \mathbf{T}_0 , \mathbf{T}_{+1} , and \mathbf{T}_{-1} :

$$\mathbf{T}_{PG,twist} = \mathbf{T}_0 + e^{i2\phi}\mathbf{T}_{+1} + e^{-i2\phi}\mathbf{T}_{-1} \quad (18)$$

where

$$\mathbf{T}_0 = \cos(X)\mathbf{R}(-\phi_{twist}) + \phi_{twist} \left[\frac{\sin(X)}{X} \right] \mathbf{R}(\pi/2 - \phi_{twist}) \quad (19a)$$

$$\mathbf{T}_{\pm 1} = e^{\pm i\phi_{twist}} \frac{\Gamma}{2} \left[\frac{\sin(X)}{X} \right] \begin{bmatrix} -i & \mp 1 \\ \mp 1 & i \end{bmatrix} \quad (19b)$$

where \mathbf{T}_m ($m = 0, \pm 1$) is a transmission matrix corresponding to the m^{th} -order of diffraction. Still, only three diffracted orders exist and the first orders have orthogonal circular polarizations regardless the incident polarization. However, the polarization state of the 0-order generally becomes elliptical due to the effect of twist.

Let us consider a Jones vector \mathbf{E}_{inc} with normalized intensity for the incoming electric field:

$$\mathbf{E}_{inc} = \begin{bmatrix} E_x \\ E_y \end{bmatrix} = \begin{bmatrix} \cos(\alpha) \\ e^{i\delta} \sin(\alpha) \end{bmatrix} \quad (20)$$

where α is an auxiliary angle ($0 \leq \alpha \leq \pi/2$) for the polarization ellipse and $\delta = \delta_y - \delta_x$ is the phase difference between E_x and E_y . The outgoing electric field of each diffracted order can be obtained as follows

$$\mathbf{E}_m = \mathbf{T}_m \mathbf{E}_{inc} \quad (m = 0, \pm 1) \quad (21)$$

Still, only three diffracted orders exist and the first orders have orthogonal circular polarizations regardless the incident polarization. However, the polarization state of the 0-order generally becomes elliptical due to the effect of twist. The normalized intensity (or efficiency) in each diffracted order is given by:

$$\eta_m = \mathbf{E}_m^\dagger \mathbf{E}_m \quad (m = 0, \pm 1) \quad (22)$$

where \mathbf{E}^\dagger denotes the Hermitian adjoint of \mathbf{E} . Diffraction efficiencies of a single Circular PG with a twist can be expressed as

$$\eta_0 = \cos^2 X + \phi_{twist}^2 \left(\frac{\sin X}{X} \right)^2 \quad (23a)$$

$$\Sigma \eta_{\pm 1} = 1 - \eta_0 = \sin^2 X - \phi_{twist}^2 \left(\frac{\sin X}{X} \right)^2 \quad (23b)$$

where $X = \sqrt{\phi_{twist}^2 + \Gamma^2}$. We omit the individual expressions for the first order efficiencies ($\eta_{\pm 1}$) because of complexity. The efficiencies can be calculated by using computer softwares such as Matlab from Eqs. 19 and 22.

Now we consider the other Circular PG with the same twist angle but opposite twist sense. Since we want to have two symmetric gratings, the anisotropy profile of two gratings should be in phase at the interface as shown in Figure 1(c) and 1(d). The Jones matrix $\mathbf{T}'_{PG,twist}$ for the second Circular PG can be obtained simply by replacing ϕ and ϕ_{twist} with $\phi + \phi_{twist}$ and $-\phi_{twist}$ from Eqs. 19, respectively:

$$\mathbf{T}'_{PG,twist} = \mathbf{T}'_0 + e^{i2(\phi + \phi_{twist})}\mathbf{T}'_{+1} + e^{-i2(\phi + \phi_{twist})}\mathbf{T}'_{-1} \quad (24)$$

and

$$\mathbf{T}'_0 = \cos(X)\mathbf{R}(\phi_{twist}) - \phi_{twist} \left[\frac{\sin(X)}{X} \right] \mathbf{R}(\pi/2 + \phi_{twist}) \quad (25a)$$

$$\mathbf{T}'_{\pm 1} = e^{\mp i\phi_{twist}} \frac{\Gamma}{2} \left[\frac{\sin(X)}{X} \right] \begin{bmatrix} -i & \mp 1 \\ \mp 1 & i \end{bmatrix} \quad (25b)$$

where \mathbf{T}_m ($m = 0, \pm 1$) is a transmission matrix corresponding to the m^{th} -order of diffraction. Since the handedness of twist does not affect the field distribution in the diffraction, the efficiencies are found same as those of the first Circular PG in Eq. 23.

The Jones matrix \mathbf{T}_{APG} for the achromatic PG (APG) composed of two chiral Circular PGs with opposite twist sense can be obtained simply by multiplying the Jones matrices for each PG:

$$\mathbf{T}_{APG} = \mathbf{T}'_{PG,twist} \mathbf{T}_{PG,twist} \quad (26)$$

Again, \mathbf{T}_{APG} can be split into three parts corresponding to each diffracted order:

$$\mathbf{T}_{APG} = \mathbf{T}_{0,APG} + e^{i2\phi} \mathbf{T}_{+1,APG} + e^{-i2\phi} \mathbf{T}_{-1,APG} \quad (27)$$

and

$$\mathbf{T}_{0,APG} = \left\{ \cos^2(X) + (\phi_{twist}^2 - \Gamma^2) \left[\frac{\sin(X)}{X} \right]^2 \right\} \begin{bmatrix} 1 & 0 \\ 0 & 1 \end{bmatrix} \quad (28a)$$

$$\mathbf{T}_{\pm 1,APG} = -ie^{\pm i\phi_{twist}} \Gamma \begin{bmatrix} \frac{\sin(X)}{X} \\ \frac{\sin(X)}{X} \end{bmatrix} \begin{bmatrix} T_{11,APG}^{(\pm)} & T_{12,APG}^{(\pm)} \\ T_{21,APG}^{(\pm)} & T_{22,APG}^{(\pm)} \end{bmatrix} \quad (28b)$$

where

$$T_{11,APG}^{(\pm)} = \cos(\phi_{twist}) \cos(X) + \phi_{twist} \sin(\phi_{twist}) \left[\frac{\sin(X)}{X} \right] \mp i [\sin(\phi_{twist}) \cos(X) - \phi_{twist} \cos(\phi_{twist})] \left[\frac{\sin(X)}{X} \right] \quad (29a)$$

$$T_{12,APG}^{(\pm)} = -\sin(\phi_{twist}) \cos(X) + \phi_{twist} \cos(\phi_{twist}) \left[\frac{\sin(X)}{X} \right] \mp i [\cos(\phi_{twist}) \cos(X) + \phi_{twist} \sin(\phi_{twist})] \left[\frac{\sin(X)}{X} \right] \quad (29b)$$

$$T_{21,APG}^{(\pm)} = -\sin(\phi_{twist}) \cos(X) + \phi_{twist} \cos(\phi_{twist}) \left[\frac{\sin(X)}{X} \right] \mp i [\cos(\phi_{twist}) \cos(X) + \phi_{twist} \sin(\phi_{twist})] \left[\frac{\sin(X)}{X} \right] \quad (29c)$$

$$T_{22,APG}^{(\pm)} = -\cos(\phi_{twist}) \cos(X) - \phi_{twist} \sin(\phi_{twist}) \left[\frac{\sin(X)}{X} \right] \pm i [\sin(\phi_{twist}) \cos(X) - \phi_{twist} \cos(\phi_{twist})] \left[\frac{\sin(X)}{X} \right] \quad (29d)$$

Interestingly, the transmission matrix for the 0-order diffraction is reduced to a identity matrix with a magnitude depending on the twist angle (ϕ_{twist}) and retardation (Γ). We can interpret that the polarization effect of twist is canceled out by two chiral layers with opposite twist sense. Therefore, the polarization of the 0-order remains same as the incident polarization.

Similar to Eqs. 23, the final expressions for diffraction efficiencies of the achromatic PG can be obtained as follows

$$\eta_0 = \left[\cos^2 X + (\phi_{twist}^2 - \Gamma^2) \left(\frac{\sin X}{X} \right)^2 \right]^2 \quad (30a)$$

$$\Sigma \eta_{\pm 1} = 1 - \left[\cos^2 X + (\phi_{twist}^2 - \Gamma^2) \left(\frac{\sin X}{X} \right)^2 \right]^2 \quad (30b)$$

where $\Gamma = \pi \Delta n d / \lambda$ and $X = \sqrt{\phi_{twist}^2 + \Gamma^2}$. We omit the individual expressions for the first order efficiencies ($\eta_{\pm 1}$) because of complexity. Again, the efficiencies can be calculated by using computer softwares such as Matlab from Eqs. 29 and 30.

REFERENCES

1. L. Nikolova and T. Todorov, "Diffraction efficiency and selectivity of polarization holographic recording," *Opt. Acta* **31**, pp. 579–588, 1984.
2. T. Huang and K. Wagner, "Coupled mode analysis of polarization volume hologram," *IEEE Journal of Quantum Electronics* **31**, pp. 372–390, 1995.
3. F. Gori, "Measuring stokes parameters by means of a polarization grating," *Opt. Lett.* **24**, pp. 584–586, 1999.
4. J. Tervo and J. Turunen, "Paraxial-domain diffractive elements with 100% efficiency based on polarization gratings," *Opt. Lett.* **25**, pp. 785–786, 2000.
5. J. A. Davis, J. Adachi, C. R. Fernandez-Pousa, and I. Moreno, "Polarization beam splitters using polarization diffraction gratings," *Opt. Lett.* **26**, pp. 587–589, 2001.
6. E. Hasman, Z. Bomzon, A. Niv, G. Biener, and V. Kleiner, "Polarization beam-splitters and optical switches based on space-variant computer-generated subwavelength quasi-periodic structures," *Opt. Commun.* **209**, pp. 45–54, 2002.
7. M. J. Escuti and W. M. Jones, "Polarization independent switching with high contrast from a liquid crystal polarization grating," *SID Symposium Digest* **37**, pp. 1443–1446, 2006.
8. H. Sarkissian, S. V. Serak, N. V. Tabiryan, L. B. Glebov, V. Rotar, and B. Y. Zeldovich, "Polarization-controlled switching between diffraction orders in transverse-periodically aligned nematic liquid crystals," *Opt. Lett.* **31**, pp. 2248–2250, 2006.
9. C. Oh and M. J. Escuti, "Numerical analysis of polarization gratings using the finite-difference time-domain method," *Phys. Rev. A*, (accepted, June 2007).
10. M. J. Escuti, C. Oh, C. Sanchez, C. W. M. Bastiaansen, and D. J. Broer, "Simplified spectropolarimetry using reactive mesogen polarization gratings," *Proc. SPIE* **6302**, p. 632614, 2006.
11. E. Collett, *Polarized Light: fundamentals and applications*, Marcel Dekker, New York, 1993.
12. H. Lajunen, J. Tervo, and J. Turunen, "High-efficiency broadband diffractive elements based on polarization gratings," *Opt. Lett.* **29**, pp. 803–805, 2004.
13. K. S. Yee, "Numerical solution of initial boundary value problems involving maxwell's equations in isotropic media," *IEEE Trans. Antennas Propag.* **14**, pp. 302–307, 1966.
14. A. Taflove and S. C. Hagness, *Computational Electrodynamics: Finite-Difference Time-Domain Method*, Artech House, Norwood, MA, 2nd ed., 2000.
15. C. Oh and M. J. Escuti, "Time-domain analysis of periodic anisotropic media at oblique incidence: an efficient fdtd implementation," *Opt. Express.* **24**, pp. 11870–11884, 2006.
16. R. C. Jones, "A new calculus for the treatment of optical systems. i. description and discussion of the calculus," *J. Opt. Soc. Am.* **31**, pp. 488–493, 1941.
17. P. Yeh and C. Gu, *Optics of Liquid Crystal Displays*, Wiley, New York, 1999.
18. J. A. Roden and S. D. Gedney, "Convolution pml (cpml): An efficient fdtd implementation of the cfs-pml for arbitrary media," *Microw. Opt. Techn. Lett.* **27**, pp. 334–339, 2000.
19. S. D. Gedney, "An anisotropic perfectly matched layer-absorbing medium for the truncation of fdtd lattices," *IEEE Trans. Antennas Propag.* **44**, pp. 1630–1639, 1996.
20. W. H. Southwell, "Gradient-index antireflection coatings," *Opt. Lett.* **8**, pp. 584–586, 1983.
21. M. G. Moharam and L. Yong, "Criterion for bragg and raman-nath diffraction regimes," *Appl. Opt.* **17**, pp. 1757–1759, 1978.
22. G. P. Crawford, J. N. Eakin, M. D. Radcliffe, A. Callan-Jones, and R. A. Pelcovits, "Liquid-crystal diffraction gratings using polarization holography alignment techniques," *J. Appl. Phys.* **98**, p. 123102, 2005.
23. C. Provenzano, G. Cipparrone, and A. Mazzulla, "Photopolarimeter based on two gratings recorded in thin organic films," *Appl. Opt.* **45**, pp. 3929–3934, 2006.
24. M. Schadt, H. Seiberle, and A. Schuster, "Optical patterning of multi-domain liquid crystal displays with wide viewing angles," *Nature* **381**, p. 123102, 1996.